Journal of Rock Mechanics and Geotechnical Engineering 9 (2017) 585–598

Contents lists available at ScienceDirect

Journal of Rock Mechanics and Geotechnical Engineering

journal homepage: www.rockgeotech.org

Full Length Article

Cyclic behavior of reinforced sand under principal stress rotation

Alaa H.J. Al-rkaby, A. Chegenizadeh*, H.R. Nikraz

Department of Civil Engineering, School of Civil and Mechanical Engineering, Curtin University, Perth, Australia

ARTICLE INFO

Article history:
Received 20 October 2016
Received in revised form
2 February 2017
Accepted 14 March 2017
Available online 12 July 2017

Keywords:
Cyclic rotation
Principal stress direction
Reinforced sand
Strain components
Damping ratio
Shear modulus

ABSTRACT

Although the cyclic rotation of the principal stress direction is important, its effect on the deformation behavior and dynamic properties of the reinforced soil has not been reported to date. Tests carried out on large-scale hollow cylinder samples reveal that the cyclic rotation of the principal stress direction results in significant variations of strain components (ε_z, ε_r, ε_θ and $\gamma_{z\theta}$) with periodic characteristics despite the deviatoric stress being constant during tests. This oscillation can be related to the corresponding variations in the stress components and the anisotropic fabric that rotate continuously along the principal stress direction. Sand under rotation appears to develop a plastic strain. Similar trends are observed for reinforced sand, but the shear interaction, the interlocking between particles and reinforcement layer, and the confinement result in significant reductions in the induced strains and associated irrecoverable plastic strains. Most of the strains occur in the first cycle, and as the number of cycles increases, the presence of strains becomes very small, which is almost insignificant. This indicates that the soil has reached anisotropic critical state (ACS), where a stable structure is formed after continuous orientation, realignment and rearrangement of the particles accompanied with increasing cyclic rotation. Rotation in the range of 60°–135° produces more induced strains even in the presence of the reinforcement, when compared with other ranges. This relates to the extension mode of the test in this range in which $\sigma_\theta > \sigma_z$ and to the relative approach between the mobilized plane and the weakest horizontal plane. Reinforcement results in an increase in shear modulus while it appears to have no effect on the damping ratio. Continuous cycles of rotation result in an increase in shear modulus and lower damping ratio due to the densification that causes a decrease in shear strain and less dissipation of energy.

1. Introduction

Reinforced soil is used widely in many geotechnical applications such as footings, embankment and pavement. In such applications, multiaxial loading and rotation in the principal stress direction are common features where the major principal stress direction is vertical for the soil element located along the load center. However, this direction rotates with α (from the vertical) when soil element is far from the centerline of the loading. Moreover, under many modes of loadings such as traffic loadings in road pavements or railways, the principal stress direction continuously rotates during moving wheel load (Ishihara and Towhata, 1983; Vaid et al., 1990; Wang et al., 2016).

It is essential to take the rotation of the principal stress direction into consideration when evaluating soil behavior, as it is found that changing not only the magnitude of the principal stress but also its direction has a significant effect on soil characteristics such as strength and deformation. This directional dependence is strongly linked to the inherent anisotropy exhibited by most soil types (Al-rkaby et al., 2016). For example, bearing capacity of footings can be reduced significantly as the principal stress direction rotates from a vertical direction (e.g. Meyerhof, 1978; Oda and Koishikawa, 1979; Azami et al., 2010). Moreover, the cyclic rotation of the principal stress direction results in significant variations of strain components, although deviatoric stress is constant during cyclic rotation (e.g. Vaid et al., 1990; Yang et al., 2007; Tong et al., 2010; Yu et al., 2016). There are many studies reported in the literature with the majority being conducted under undrained conditions (Ishihara and Towhata, 1983; Nakata et al., 1998; Yang et al., 2007) or under monotonic rotation of the principal stress direction (Symes et al., 1988; Wijewickreme and Vaid, 1993; Jiang et al., 2012; Cai et al., 2013). In addition, there are some studies performed to

* Corresponding author.
E-mail address: amin.chegenizadeh@curtin.edu.au (A. Chegenizadeh).
Peer review under responsibility of Institute of Rock and Soil Mechanics, Chinese Academy of Sciences.

http://dx.doi.org/10.1016/j.jrmge.2017.03.010

examine the cyclic rotation of the principal stress direction under drained conditions (e.g. Tong et al., 2010; Yu et al., 2016). However, all of these studies were limited to plain soil and did not investigate reinforced soil under cyclic rotation, despite the wide use of reinforced soil structure.

The hollow cylinder apparatus (HCA) was used to investigate soil characteristics under continuous cyclic rotation instead of the conventional triaxial test that could not simulate this condition. One reported study using plain sand found periodic variations in the induced strains due to the rotation of the principal stress direction and the majority of these strains were generated during the first cycle (Yu et al., 2016). These strains resulted in dilation and contractive volumetric strain during the rotation of the principal stress direction from 0° to 180°. However, at the end of each cycle, the total strain was contractive. Similar results were found by Xiong et al. (2016) using sand under the rotation of the principal stress direction resulting in plastic irrevocable strains. The shear strain reached its maximum value at $\alpha = 60°$ and then decreased until $\alpha = 150°$, while the axial strain induced in dilation side reached the maximum at $\alpha = 120°$. Most of the induced volumetric strain took place in the first cycle and this strain varied significantly along α. With the subsequent cycles, it was generated at a low rate but the variation along α became insignificant due to the densification of soil (Tong et al., 2010; Xiong et al., 2016). These induced strains were also observed using a pure rotation test by Cai et al. (2013), although the intermediate principal stress ratio (b) was not constant along the rotation and only one cycle was considered.

The cyclic rotation under undrained conditions has a significant effect on soil behavior where flow deformation took place and more than 5% of pore pressure and strains were accumulated under constant deviatoric stress and b of 0.5 (Nakata et al., 1998). Similar trends were reported by Yang et al. (2007) under undrained conditions. Constant b and deviatoric stress increased the pore water pressure significantly due to cyclic rotation and most of it occurred during the first cycle. They observed that the generated pore pressures varied along α during the first cycle. However, in the subsequent cycles, the increasing rate tended to slow down and the variation along α became insignificant.

The dynamic characteristics of soil, such as the shear modulus and damping ratio, are of significant importance to analyze soil behavior and assess many geotechnical projects that involve a cyclic component (RaviShankar et al., 2005). These dynamic properties are affected by anisotropic fabric (Qin et al., 2015).

Few studies are reported in the literature regarding the dynamic properties of soil under cyclic rotation. Tong et al. (2008, 2010) found that the shear modulus increased as cyclic rotation continued.

Of the reported studies that did not consider the rotation of the principal stress direction, Naeini and Gholampoor (2014) examined the damping ratio for reinforced sand using a variety of numbers and places of geotextile under a normal cyclic test and found that the geotextile had no effect on the damping ratio. Moreover, in contrast to the findings of Tatsuoka et al. (1978), who suggested that there was no clear effect of void ratio on damping ratio, Kirar and Maheshwari (2013) demonstrated a decrease in the damping ratio and an increase in the shear modulus that are related to density increase. This is in agreement with Uthayakumar (1992) who concluded that a lower damping ratio, when the void ratio decreased, was associated with stiff material which dissipated lower amounts of energy during the cyclic loading.

It is apparent that the cyclic rotation has a very important effect on the deformation behavior of soil in many geotechnical problems, and should be considered in any design. Although reinforcement is widely used in many geotechnical applications to support the applied stress, the behavior of reinforced sand under cyclic rotation of the principal stress direction has not been reported in the literature to date. For this, experiments on large-size samples of geogrid-reinforced sand under cyclic rotation of the principal stress direction have been undertaken in this study. Additionally, the dynamic properties of reinforced sand under such conditions are investigated. This study is part of an ongoing research study at Curtin University and there are other aspects of this study yet to be investigated (Al-rkaby et al., 2017).

2. Materials and methods

2.1. Soil and geogrid

The sand used in this study was bought from Perth, Australia. It is classified as poorly graded sand (SP) and Table 1 shows some of its properties. Fig. 1 shows the particle size distribution of the sand used. High-density polyethylene geogrid was used for reinforcement and its properties are shown in Table 2.

2.2. Large hollow cylinder apparatus

The rotational cyclic tests were conducted using an advanced large HCA (HCA-600) at Curtin University. This apparatus can accommodate large samples with outer diameter $D_o = 300$ mm, inner diameter $D_i = 150$ mm and height $H = 600$ mm (Fig. 2). Despite the difficulties of handling such large samples, it can provide reliable and more accurate representation of soil deformations, especially under anisotropic conditions.

This device is useful for studying the anisotropic behavior of soil to consider different geotechnical problems that could not be simulated in a conventional triaxial apparatus, such as the effect of the rotation of the principal stress direction under a reasonably generalized stress state. Moreover, different directions of principal stress (α) or continuous rotation of the principal stress direction and various relative magnitudes of the intermediate principal stress ratio (b) can be achieved by the capability of independently controlling the axial load (W_z), torque (M_T), outer cell pressure (p_o), and inner cell pressure (p_i), resulting in individual control of the four stress components acting on an element (Fig. 2), i.e. vertical stress (σ_z), radial stress (σ_r), circumferential stress (σ_θ), and shear stress ($\tau_{z\theta}$).

2.3. Sample preparation

Sand was poured into samples and tamped as layers with a relative density of about 70%. Reinforcement geogrid with inner and outer diameters less than those of samples was placed in 2–5 layers at equal distance.

Table 1
Physical properties of the sand used.

Coefficient of uniformity	Coefficient of curvature	D_{30} (mm)	Medium grain size (mm)	D_{60} (mm)	Maximum void ratio	Minimum void ratio	Specific gravity	USCS classification	Friction angle (°)	Cohesion (kPa)
1.5	1.04	0.5	0.6	0.603	0.826	0.549	2.65	SP	40.1	0

Note: D_{30} and D_{60}: the sizes such that 30% and 60% of the particles are smaller than those sizes, respectively; USCS: unified soil classification system.

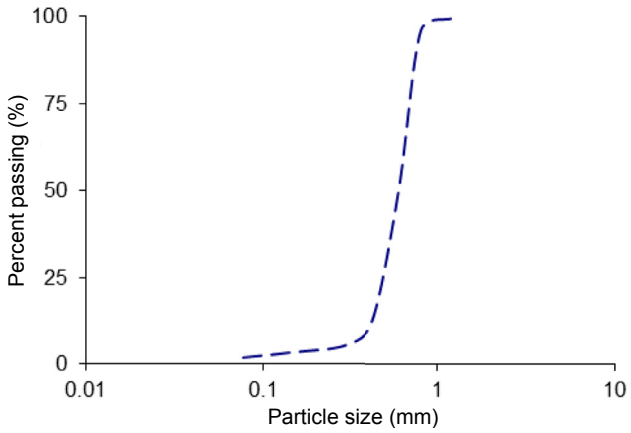

Fig. 1. Grain size distribution of the sand used.

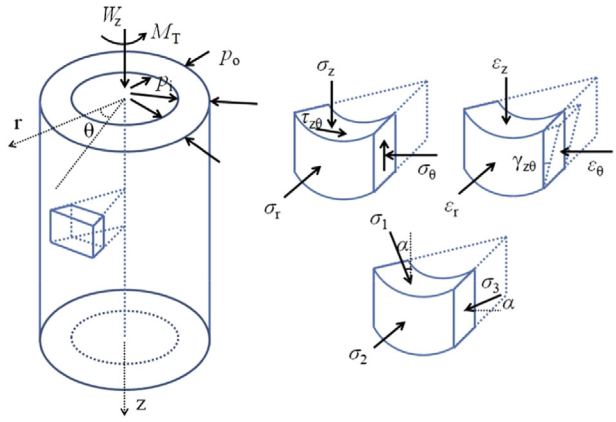

Fig. 2. Stress state of hollow cylinder samples (Guo et al., 2016). θ is the torsional angle; σ_1, σ_2 and σ_3 are the major, intermediate and minor principal stresses, respectively; ε_r, ε_θ, ε_z and $\gamma_{z\theta}$ are the radial, circumferential, axial and shear strains, respectively.

The large size of the hollow samples and the heavy accessories required special attention during the preparation process due to safety concerns. Thus, the preparation process required at least three people and a forklift to install the samples. Experience in handling large samples was necessary during preparation and installation of the samples, and it was suggested to test some samples before starting the experiments. For example, a great care had to be taken using a forklift to lower the large cell chamber in order to avoid knocking of the side and top of the sample which may cause some disturbance to the sample. Moreover, the space between the actuator and connector is small resulting in difficulty in fixing the sample to the actuator (Al-rkaby et al., 2017). Selected photos of the preparation process are summarised in Fig. 3.

After the sample had been set up in the cell using vacuum pressure, a procedure similar to that described by Miura et al. (1986), Razeghi and Romiani (2015), Yang et al. (2015), Xiong et al. (2016), and Yu et al. (2016) was used where the saturation process was carried out after filling the inner and outer chambers with degassed water. Saturation was achieved by applying different levels of back pressure while the initial effective stress was kept constant at 30 kPa for about 12 h, in order to achieve a Skempton's *B*-value greater than 0.95. Then the isotropic consolidation stage was conducted by increasing the effective confining pressure (inner and outer) to 100 kPa.

2.4. Testing program

Two series of rotational cyclic tests were performed on the sand samples in this study (Table 3) to investigate the effect of the rotation of the principal stress direction on the soil behavior. The first series of tests was performed on unreinforced samples of Perth sand under a constant stress ratio and continuous rotation of the principal stress direction. The second series of tests was performed on reinforced sand under similar conditions. Reinforced and unreinforced samples were saturated to obtain a *B* value of more than 0.95, and then consolidated isotropically before the cyclic rotation commenced. In both series, initial relative density was 70% and the intermediate principal stress ratio (b) was constant (0.5) during cyclic rotation. The principal stress direction was rotated from 0° to 180° and lasted for 60 cycles. The rate of rotation was controlled at 2° per minute to allow the full discharge of water from samples during test, as described by Yu et al. (2016). During the stress path of the tests (Figs. 4 and 5), the samples are sheared under a constant deviatoric stress (q) and mean effective stress (p') of 60 kPa and 100 kPa, respectively, i.e. stress ratio ($R = q/p'$) of 0.6 after consolidation to point *A*, and then the principal stress rotated counterclockwise from 0° to 180° following the circular cyclic path from *A* to *B*, *C*, *D* and then *A*. During the rotation of the principal stress direction, axial stress (σ_z), circumferential stress (σ_θ) and shear stress ($\tau_{z\theta}$) varied with oscillation mode while the mean effective stress (p'), deviatoric stress (q), intermediate principal stress ratio (b), major principal stress (σ_1), intermediate principal stress (σ_2) and minor principal stress (σ_3) were kept unchanged (Fig. 6). Sixty cycles in total were performed in each rotation test using both reinforced and unreinforced sands. Similar studies have been reported by Miura et al. (1986), Tong et al. (2008, 2010), Xiong et al. (2016) and Yu et al. (2016).

3. Results and discussion

3.1. Unreinforced sand

Fig. 7 shows the variations of strain components with the number of cycles and the principal stress direction during the rotation of the principal stress direction. Positive and negative signs indicate compression and dilation, respectively. It is evident that although the deviatoric stress was kept constant during the test, significant vertical (ε_z), radial (ε_r), circumferential (ε_θ) and shear ($\gamma_{z\theta}$) strains were generated, indicating a significant effect of the rotation of the principal stress direction on the deformation behavior of the sand.

Table 2
Physical properties of geogrid.

Model	Material	Mesh aperture (mm × mm)	Weight per unit area (N/m^2)	Ultimate tensile strength (kN/m)		Stiffness (kN/m)	
				Machine direction	Transversal direction	Machine direction	Transversal direction
CE121	High-density polyethylene	8 × 6	7.15	9.8	6.15	68	60

Fig. 3. Sample preparation and installation (Al-rkaby et al., 2017). (a) Seat the pedestal base (with porous stone and inner membrane) on the bottom base and bolt them. (b) Sample before placing the geogrid layer. (c) Preparing the geogrid layer. (d) Place a geogrid layer on the sand layer in sample. (e) Prepared sample. (f) Bring down the cell chamber with special care and tighten it. (g) Use forklift to lift the prepared sample and set it up in the apparatus.

In Fig. 7b, an increase of the shear strain ($\gamma_{z\theta}$) can be observed from the beginning of the rotation, reaching the maximum value at $\alpha = 73^\circ$ then decreasing to zero as α increases to 115°. Further increasing of α results in the shear strain reaching its lowest value at around 137°, and then increasing slightly until the end of cycle. However, it does not return to the initial value before rotation. The circumferential strain (ε_θ) increases slightly with rotation. However, when α approaches 40°, a significant increase of ε_θ occurs with a maximum value at $\alpha = 105^\circ$, then ε_θ decreases and still remains on the compression side. A similar trend is observed for ε_r, however, its variation along α is less than the variation of ε_θ along α. For the axial strain (ε_z), a clear dilation behavior is recorded where ε_z increases slightly from the beginning of rotation until $\alpha = 30^\circ$–40° when a dramatic increase of dilation occurs, reaching its maximum value at $\alpha = 105^\circ$ then decreasing steadily until the end of the cycle ($\alpha = 180^\circ$) and remaining dilated.

All strain components at the end of the cycle do not return to their initial values before starting the rotation, although the stress components do return back to their initial state. This shows that plastic strains occur and lead to irrecoverable deformation (Fig. 7). This plastic strain can also be seen in the spiral curve of strain path in deviatoric strain space (ε_z–ε_θ) vs. $2\gamma_{z\theta}$ (Fig. 8). In this strain path, when plastic deformation occurs, the stress path forms an open space and the vector from the start point to the end point of each single cycle represents the amount of irrecoverable strain (Li et al., 2016; Yu et al., 2016). The largest plastic strain can be observed in the first cycle. However, with continuous rotation, the open space tends to be closed indicating a small amount of plastic deformation.

During the subsequent cycles of the rotation of the principal stress direction, it can be observed that most of the strains are produced during the first cycle (Fig. 7). Subsequently, ε_z reduces moderately within the first five cycles followed by a slight decrease as the number of cycles N increases. The circumferential strain (ε_θ) increases slightly as the number of cycles increases, but ε_r increases significantly until $N = 20$ and then the increasing rate decreases. For example, the axial strain, ε_z, increases to −0.39% after the first

Table 3
Summary of the rotational tests.

Test No.	Stress ratio q/p'	Intermediate principal stress ratio, b	Number of geogrid layers	Principal stress direction, α
1	0.6	0.5	Unreinforced samples	Rotation from 0° to 180° for 60 cycles
3	0.6	0.5	2, 3, 4 and 5	Rotation from 0° to 180° for 60 cycles

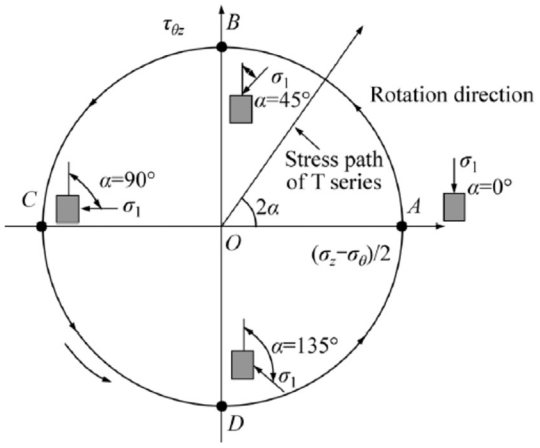

Fig. 4. Typical stress path in deviatoric space for rotational shear test (Yan et al., 2015).

rotation cycle and then decreases to −0.347% and −0.345% after 30 and 60 cycles, respectively. Circumferential strain (ε_θ) increases to 0.322% during the first cycle and increases as N increases to 0.4% and 0.466% after 30 and 60 cycles, respectively. This is in agreement with studies reported by Tong et al. (2008, 2010), Xiong et al. (2016) and Yu et al. (2016).

The variations in strain components can be explained by the connection to the variation in the stress state where the sample, with inherent anisotropy due to the preferred orientation of particles, is subjected to axial stress vertically before starting rotation, in which vertical stress (σ_z) and circumferential stress (σ_θ) are the major and minor principal stresses, respectively (Yang, 2013; Yan et al., 2015). This results in the sample in horizontal direction having higher compressibility and lower dilation compared to the

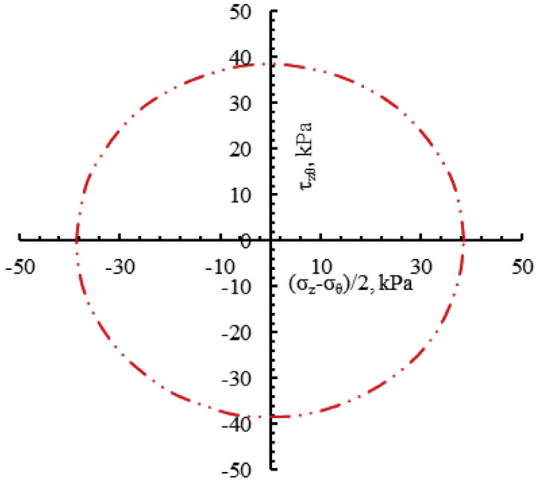

Fig. 5. Typical stress path of test under rotational condition.

vertical direction (Yang, 2013; Yan et al., 2015). Once the rotation begins, σ_z decreases while σ_θ increases (Fig. 6a and b). The resulting deformation is in the form of contraction along the circumferential direction, and the plane is most susceptible to deformation. Sand subjected to cyclic rotation will develop an anisotropic structure due to the capability of the granular material to rearrange its internal structure to achieve mechanical stability when sheared. This anisotropic fabric will rotate continuously in the direction of the principal stress with a few degrees of lag and consequently result in accumulated strains that have varied oscillation characteristics (Li and Yu, 2010; Yu et al., 2016).

The volumetric strain is presented in Figs. 9 and 10 where the positive values indicate compression behavior. It accumulates as the number of cycles increases, although the deviatoric stress ratio q/p' is constant throughout the cyclic rotation and most of the induced ε_v occurs during the first cycle, and then the increasing rate tends to reduce (Fig. 9). Similar trend was observed by Tong et al. (2008) and Yu et al. (2016), as shown in Fig. 9. During the first five cycles, the volumetric strain is contractive along α with a slight dilation occurring at the 4th and 5th cycles. With the increasing number of cycles, the variation of ε_v along α becomes smaller with some dilation (Fig. 10).

This dilation is likely to be attributed to the densification of sample occurring during the previous cycles of rotation. Although both contraction and dilation occur in the tested samples during the individual cycle, the contractive behavior is dominant on the accumulated volumetric strain at the end of each cyclic rotation. This agrees with the findings of Xiong et al. (2016) who reported that sand became denser by 12% after 20 cycles of rotation.

It is noted that fabric anisotropy can considerably affect the deformation behavior of sand, particularly in the first cycle of the rotation of the principal stress direction. However, in the subsequent cycles, the initial fabric anisotropy can be destroyed because of the induced shear deformation resulting from cyclic rotation. On the other hand, the results obtained from this study demonstrate that the development and oscillation of the accumulated strain components tend to decrease significantly after the first cycle (Figs. 7 and 10). This may be attributed to the property of soil that can achieve some stability of structure after continuous orientation, realignment and rearrangement of particles accompanied with increasing cyclic rotation. This is consistent with the anisotropic critical state (ACS) proposed by Li and Dafalias (2012) where soil becomes independent of initial fabric anisotropy, unless severe particle breakage occurs. Similar observation of this critical state and the destruction of the initial anisotropic fabric has been reported by Oda and Koishikawa (1979), Sazzad and Suzuki (2010), Fu and Dafalias (2011), Fonseca et al. (2013) and Tong et al. (2014). This destruction of initial anisotropy can be recognized by the significant drop in the frequency of particles oriented along a specific angle α after loading, when compared to the initial state, as observed by Hosseininia (2012).

This reduction in the development and oscillation of the accumulated strain components also corresponds to a process of loss and creating contact in the anisotropic fabric occurring as the cycles increase, where the occurrence of plastic strain in the sand sample results in loss of existing fabric contact and the generation of new contacts and consequently leads to continuous change in the contact fabric. This change in fabric is related to the fabric anisotropy of granular material which can be recognized from the orientation of the normal contact distribution (Sazzad and Suzuki, 2010). In the inherent anisotropic structure, the elongated particles prefer to align horizontally and thus exhibit the greatest stability to vertical stress but the stability becomes less under inclined stress. Therefore, particles tend to rotate to support the rotation of the principal stress direction, which rotates continuously. As a consequence,

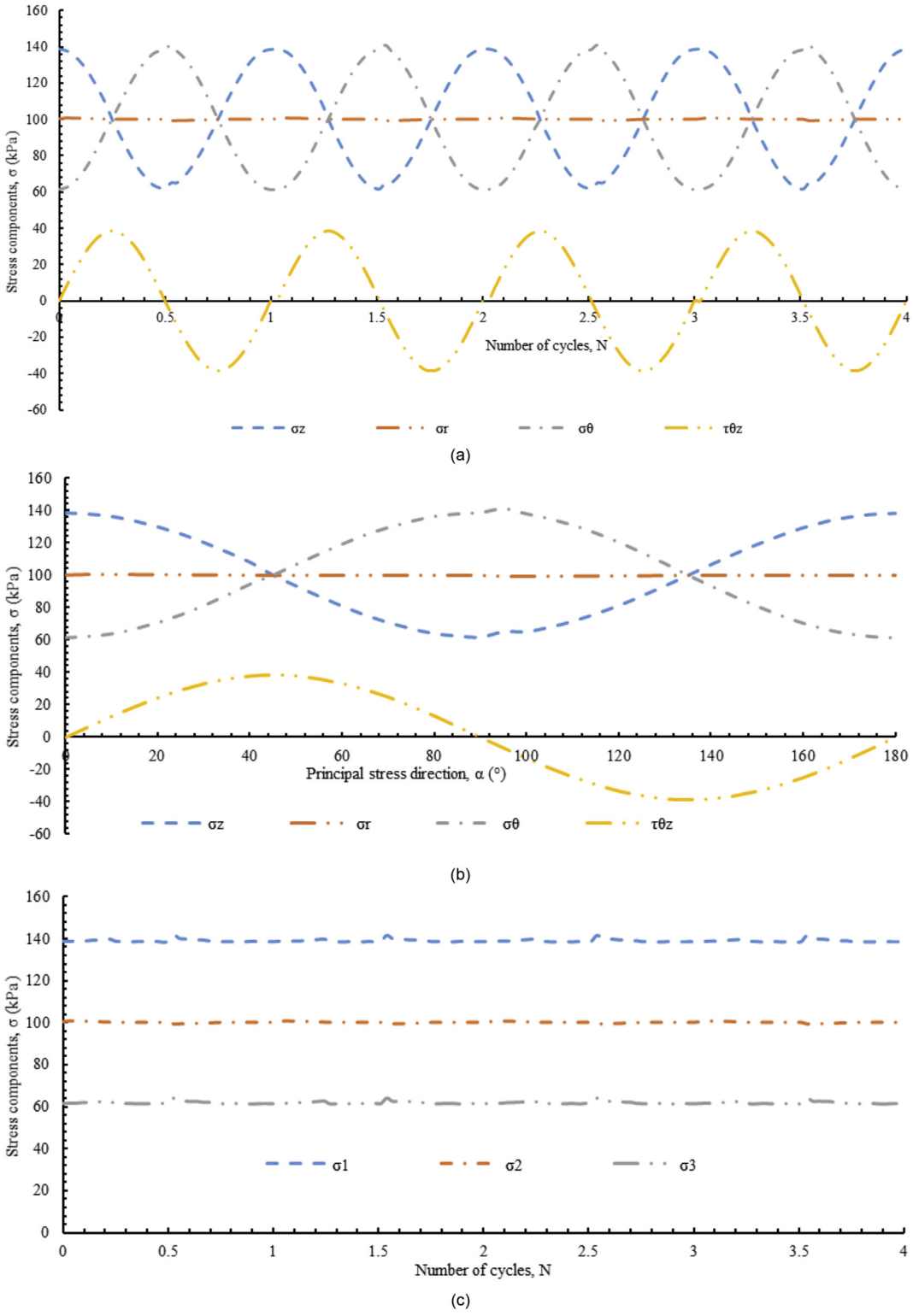

Fig. 6. (a) Typical variations of stress components (σ_z, σ_θ, σ_r, $\tau_{z\theta}$) during the first four cycles. (b) Typical variations of stress components (σ_z, σ_θ, σ_r, $\tau_{z\theta}$) along the principal stress direction (α) during single cycle. (c) Typical variations of principal stresses (σ_1, σ_2, σ_3) during the first four cycles.

more normal contacts will be lost during cycles and the preferred direction of the contact anisotropy tends to rotate towards the principal direction. The change in fabric anisotropy is significant during the first few cycles and then becomes steady, indicating that fabric might approach the critical state after many cycles of accumulated reorientation and the contact fabric will change.

3.2. Reinforced sand

Fig. 11 shows the deformation behavior of sand reinforced with geogrid under cyclic rotation. It is clear that the reinforcement plays a significant role in decreasing all four strain components. Circumferential and radial strains decrease significantly for 3–5

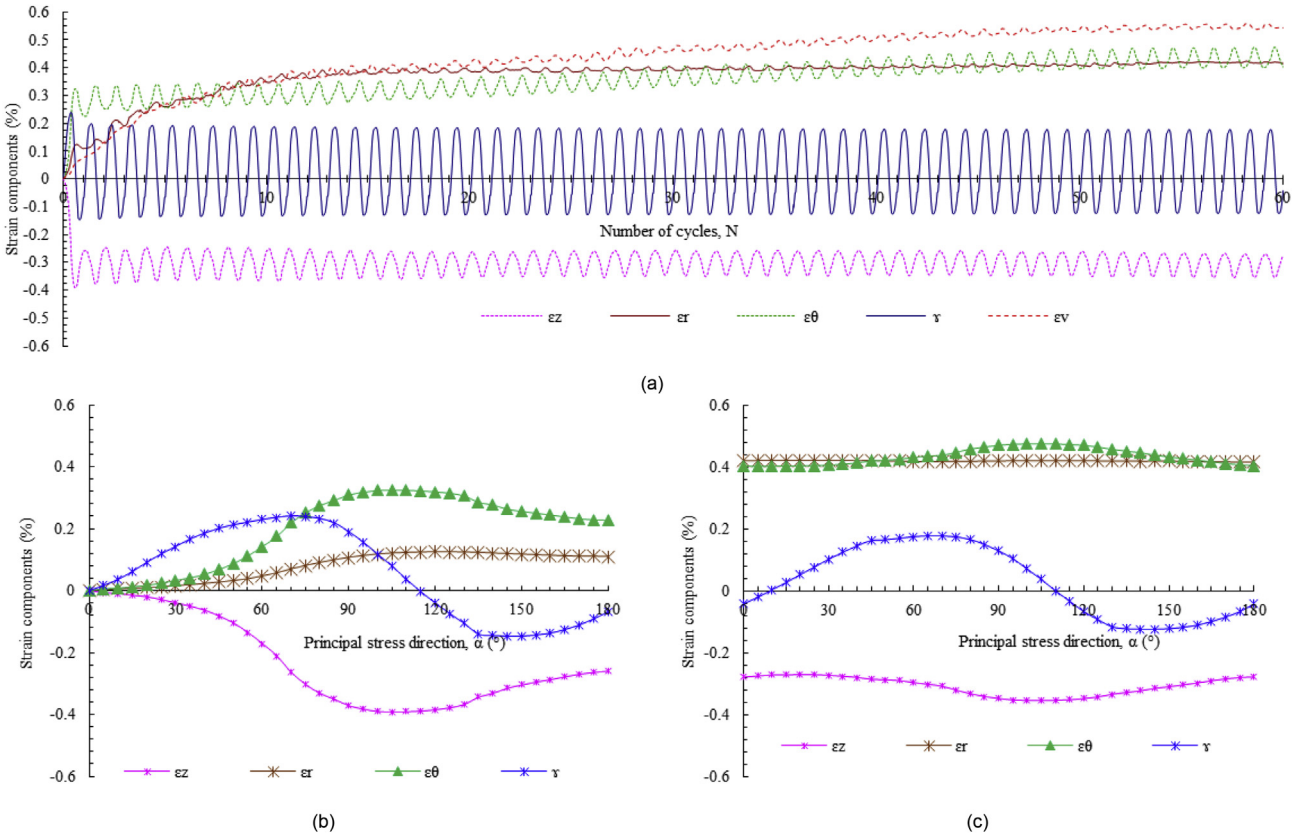

Fig. 7. (a) Development of strain components (ε_z, ε_r, ε_θ, $\gamma_{z\theta}$) and volumetric strain (ε_v) of unreinforced sand with number of cycles during the rotation of the principal stress direction. (b) Strain components (ε_z, ε_r, ε_θ, $\gamma_{z\theta}$) of unreinforced sand in the first cycle of rotation along the principal stress direction. (c) Strain components (ε_z, ε_r, ε_θ, $\gamma_{z\theta}$) of unreinforced sand in the 60th cycle of rotation along the principal stress direction.

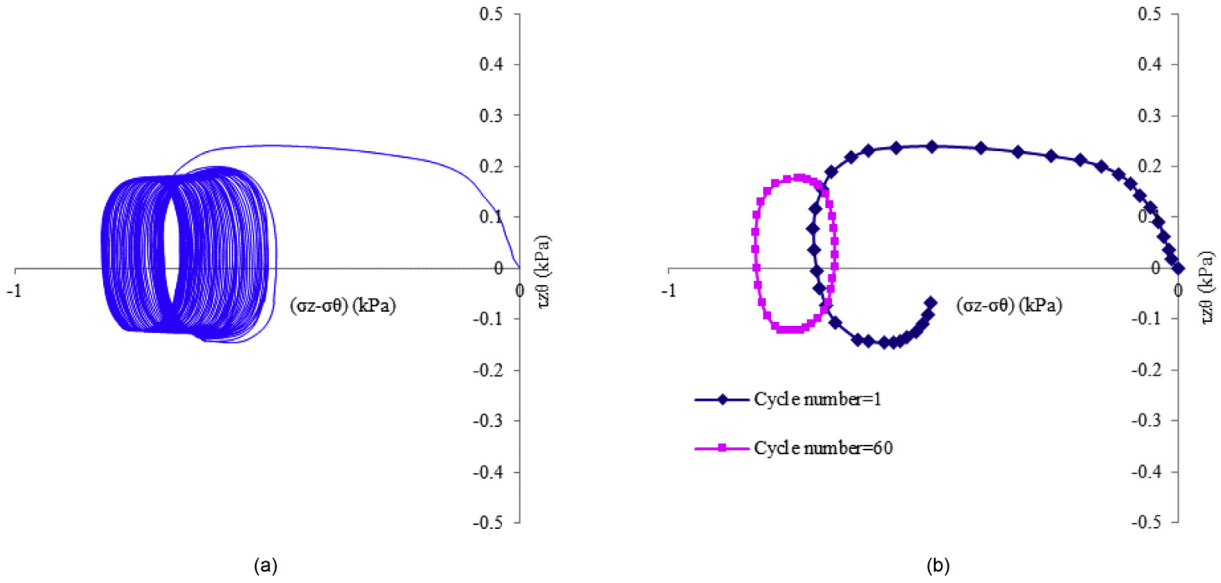

Fig. 8. Strain paths of unreinforced sand in deviatoric strain space for (a) cyclic rotation and (b) the first and 60th cycles.

layers. However, axial strain exhibits a small decrease when compared to ε_r and/or ε_θ. A moderate decrease is observed in the shear strain. The volumetric strain ε_v is accumulated as the number of cycles increases and most of the induced ε_v occurs during the first cycle, and then it is generated at a low rate (Figs. 12 and 13). During the first five cycles, the volumetric strain is contractive along α. With the subsequent cycles, a slight dilation occurs and the variation of ε_v along α becomes insignificant (Figs. 12 and 13). It can be observed that the amount of volumetric strain of reinforced sand with 5 layers, for example, and its variation along α are much less compared with those of unreinforced sand. However, reinforcement with 2 layers does not show a significant effect.

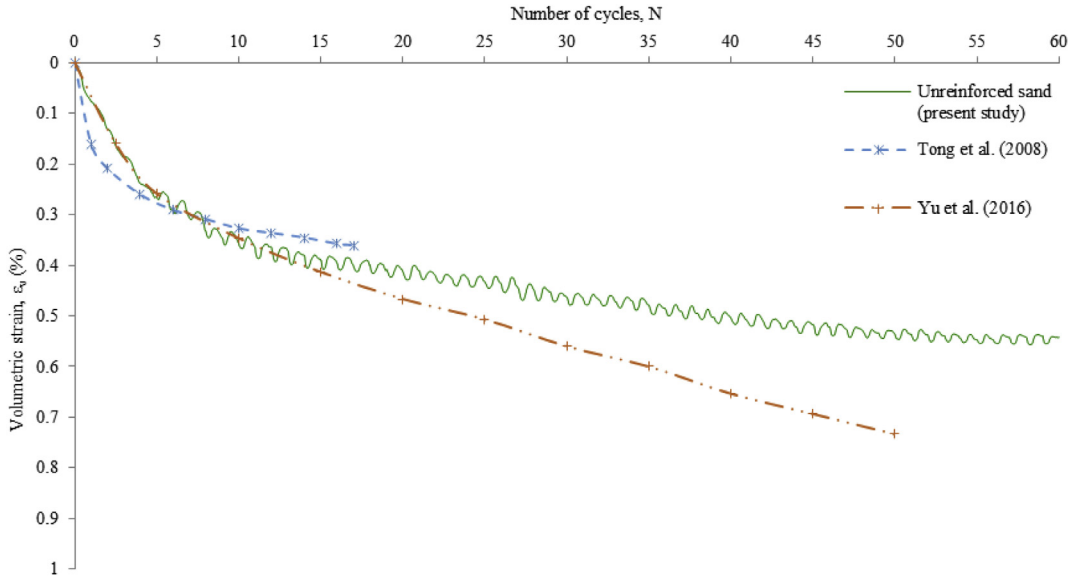

Fig. 9. Evolution of volumetric strain (ε_v) of unreinforced sand due to cyclic rotation compared with available previous studies.

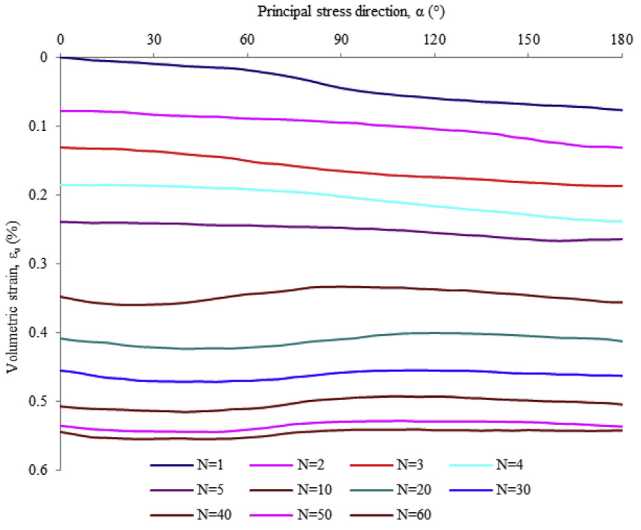

Fig. 10. Variations of developed volumetric strain (ε_v) of unreinforced sand along the principal stress direction (α) at different numbers of cycles.

The oscillation characteristics of strains are linked to the variation of the applied stresses while the observed reduction in the induced strains is attributed to the mechanism of the reinforcing of the geogrid, which can provide an internal confinement. This confinement varies depending on the tensile strength of the geogrid, friction between the sand and geogrid at the interface, and the induced stress of sand confined in the geogrid apertures due to passive resistance provided by the reinforcement.

Before the rotation, the sample is under an axial stress, resulting in an axial deformation and subsequently increasing the interaction between the geogrid and sand. This induces a radial strength in geogrid which resists the lateral deformation generated in sample. Therefore, the sample has a relatively low compressibility in both the axial and horizontal directions. The variation of strain components is likely to be related to the variation of the stresses (Fig. 6a and b). For rotation in the range between $\alpha = 0°$ and 45°, σ_z still remains greater than σ_θ, although σ_z starts to decrease and σ_θ increases, resulting in a dilation in the vertical direction and a slight contraction in circumferential direction. Within this range, the applied vertical stress contributes to more interaction between the sand and geogrid, resulting in restriction in the lateral strain. With continued rotation in the range between $\alpha = 45°$ and 90°, σ_z decreases further, σ_θ increases and the condition changes to $\sigma_\theta > \sigma_z$. Consequently, the interaction becomes less, resulting in a clear lateral contraction. However, this contraction was less compared with that of unreinforced sand. The subsequence rotation (90°–135°) shows that σ_z increases and σ_θ decreases, noting that σ_θ remains larger than σ_z and this increase in σ_z provides more interaction between the geogrid and sand. This can restrain the contractive lateral deformation and decrease the dilation in the vertical direction. For the remaining range of rotation ($\alpha > 135°$), σ_z becomes larger than σ_θ, resulting in more interaction and consequently higher restraint. This means that although the cyclic rotation still induces a clear deformation, reinforcement can result in restriction in the radial and circumferential strains. This restraint becomes more evident in the subsequent cycles due to the densification and stress history that lead to advanced interaction between the sand particles and geogrid layers. It should be mentioned that reinforced sand with 2 layers shows insignificant resistance to rotation.

The improvement of deformation behavior can be explained based on the sand geogrid interaction that may include the mechanisms of (a) shear resistance between the sand and surface of the geogrid ribs and surrounding soil, and (b) internal shear resistance of the particles inside the aperture (Liu et al., 2009). Moreover, the normal stress on reinforced sand results in an increase in the frictional resistance and therefore, the observed lower level of volumetric strain (radial and circumferential strains) in reinforced sand can be explained by that, when materials are loaded, lateral deformation is likely to develop in alignment with the direction of the reinforcement layers. The inclusion of a geogrid will result in shear interaction and interlocking forces between particles and the reinforcement layer as mentioned in the above mechanism. These shear stresses will be transmitted from the sand particles to the geogrid, which will come under tension where the tensile strain is induced, resulting in a tensile stress along the reinforcement. The geogrid will resist this induced tensile stress

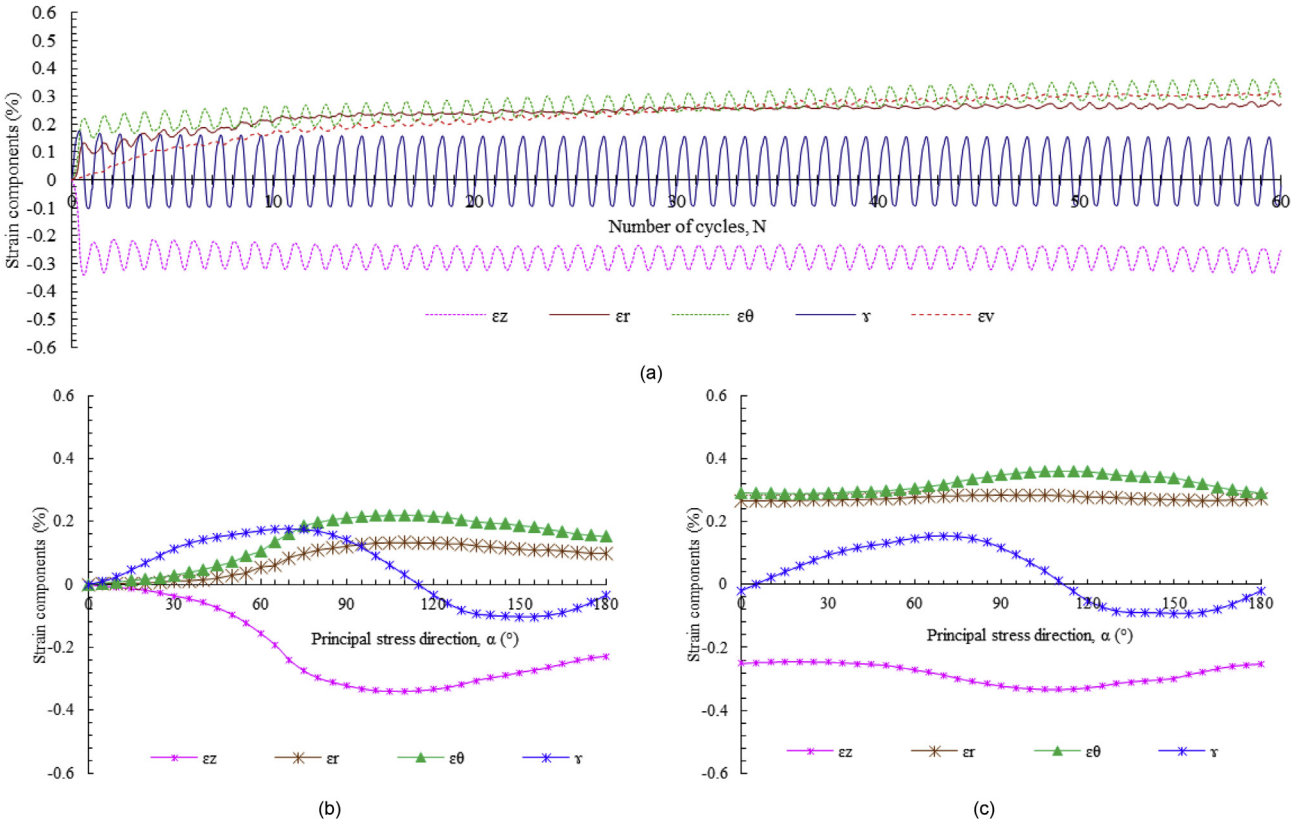

Fig. 11. (a) Development of strain components (ε_z, ε_r, ε_θ, $\gamma_{z\theta}$) and volumetric strain (ε_v) of 5-layer reinforced sand with number of cycles during the rotation of the principal stress direction. (b) Strain components (ε_z, ε_r, ε_θ, $\gamma_{z\theta}$) of 5-layer reinforced sand in the first cycle of rotation along the principal stress direction. (c) Strain components (ε_z, ε_r, ε_θ, $\gamma_{z\theta}$) of 5-layer reinforced sand in the 60th cycle of rotation along the principal stress direction.

and strain by the mobilization of the tensile stress, the confinement and interaction of the geogrid reinforcement to the surrounding soil. This will consequently restrict the development of lateral tensile strains (lateral expansion) in the sand adjacent to the geogrid layer. This restriction will decrease the level of dilation motivation and increase the strength. As the reinforcement layers increase, there will be greater confinement and interaction, thus greater resistance to lateral deformation occurs. This is consistent with the findings of Higuchi et al. (1998), Peng et al. (2000), Nazzal et al. (2007) and Liu et al. (2014).

The spiral curve of the strain path (Fig. 14) shows that there is an induced plastic strain particularly during the first cycle in which the space is open, followed by a smaller amount of irrecoverable deformation in which the space of each cycle tends to be closed.

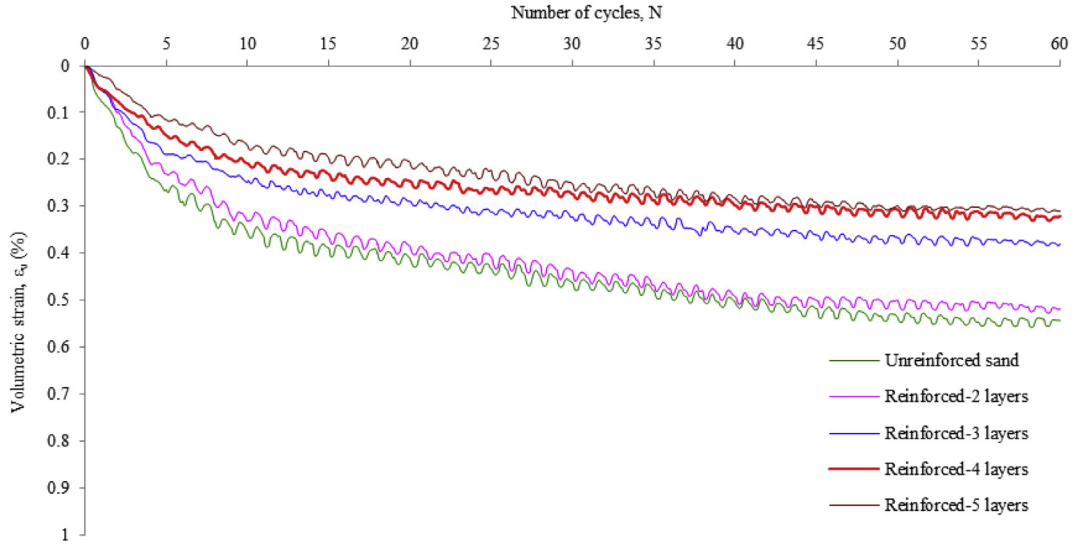

Fig. 12. Evolutions of volumetric strain (ε_v) of reinforced sand due to cyclic rotation.

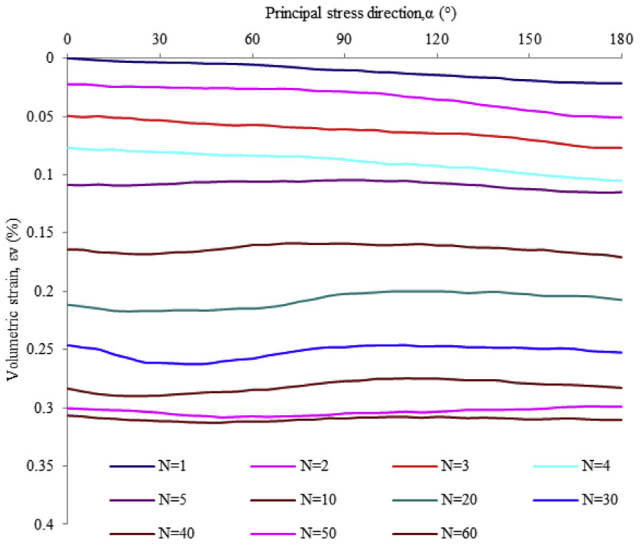

Fig. 13. Variations of developed volumetric strain (ε_v) of 5-layer reinforced sand with the principal stress direction (α) at different numbers of cycles.

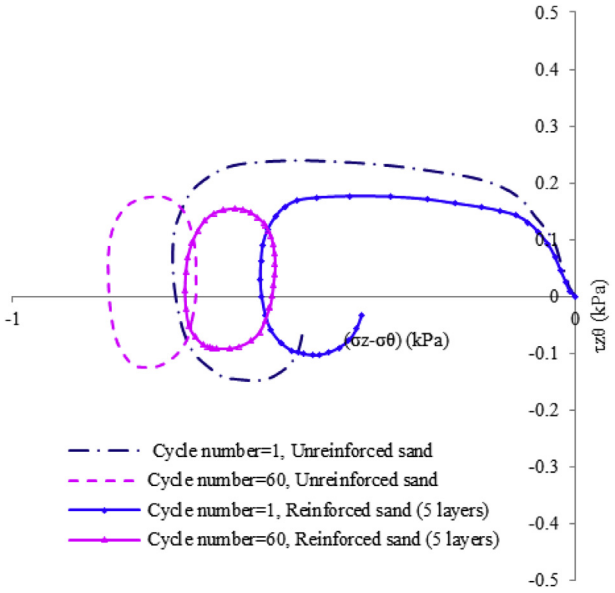

Fig. 15. Comparisons of the strain paths in deviatoric strain space of the first and 60th cycles between unreinforced and 5-layer reinforced sands.

This trend is similar to that described in the previous section. However, this induced plastic strain is much lower than that of the unreinforced sand, as compared in Fig. 15.

During the rotation from 45° to 135°, induced strains are clearly observed despite the presence of geogrid as reinforcement compared with the other range of rotation (e.g. Figs. 11b, c and 12). This can be related to samples entering some extension mode throughout this range, in addition to the relative approach between the mobilized plane and the bedding plane, as will be explained hereafter. For the range of $\alpha = 45°–135°$, the ability of geogrid layers laid horizontally to resist shearing decreases significantly when the direction of the principal stress changes towards the horizontal plane. During this range of rotation, samples are sheared in some extension mode, and the axial stress (σ_z) becomes smaller than the circumferential stress (σ_θ). This may give an explanation for the observed induced strains where reinforced sand under $\sigma_\theta > \sigma_z$ (case of $\alpha = 45°–135°$) does not exhibit enough restraint and confinement, compared with those when $\sigma_z > \sigma_\theta$. This means that the geogrid reinforcement under some extension conditions does not provide similar resistance to that observed under compression. Moreover, the induced strain caused by the rotation in the range of 45°–135°, even with reinforcement, can also be linked to the relative approach between the mobilized plane and the horizontal plane, characterised as the weakest plane. This weakness of the horizontal bedding plane is due to the tendency of elongated particles aligning horizontally, resulting in poor interlocking, easy sliding and consequently reducing the maximum deformation and minimum strength. The potential mobilized plane makes an angle of $(45° - \phi/2)$ on both sides of the principal stress, where ϕ is the angle of internal friction of the soil. Therefore, a rotation in the range of $\alpha = 45°–135°$ moves the mobilized plane closer to the weakest horizontal plane and this results in a less effective reinforcement. Similar trend of reinforced sand response to the principal stress direction has been reported by Habibi et al. (2014) and Al-rkaby et al. (2017) but under monotonic tests.

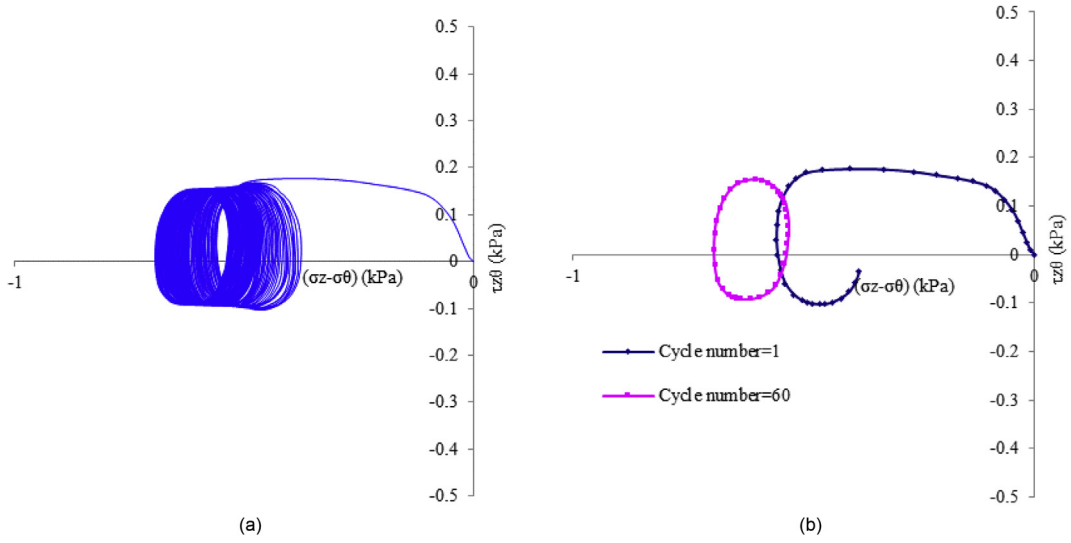

Fig. 14. Strain paths of 5-layer reinforced sand in deviatoric strain space for (a) cyclic rotation and (b) the first and 60th cycles.

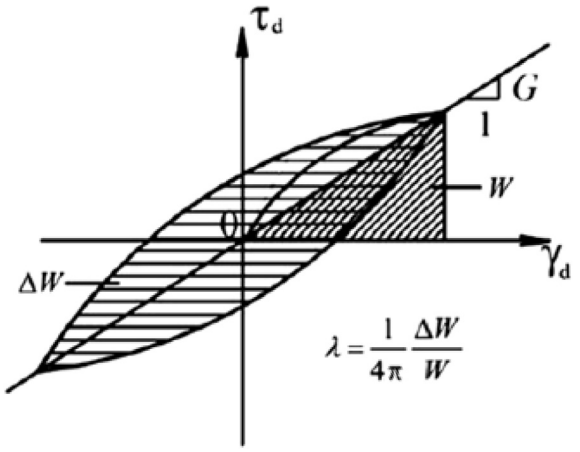

Fig. 16. Typical hysteresis loop representing the relationship between shear strain and shear stress (Wang et al., 2012). W is the area of hatched triangle and represents the maximum elastic energy stored in the same loading cycle, ΔW is the area enclosed by the hysteresis loop and represents the energy dissipated during the loading, λ is the damping ratio, τ_d is the shear stress, and γ_d is the shear strain.

Although the aim of these tests was to study the anisotropic deformation and dynamic properties of reinforced sand as a composite material under cyclic rotation of the principal stress direction, some tests (sample reinforced with 2 and 5 layers) were carried out to investigate the mobilized stress of reinforcement. However, measuring the deformation of reinforcement inside a triaxial apparatus is very complex and only Chandrasekaran et al. (1989), Nguyen et al. (2013) and Liu et al. (2014) have tried to do so. Similarly to Nguyen et al. (2013), we implement these extra tests to compute mobilized stress in reinforcement which depends on measuring the plastic deformation that could be induced in the reinforcement. During the tests, a significant amount of strain is induced in the reinforced sample (as a composite material) similar to what we previously presented. This is because the soil deforms easily compared to the geogrid where particles tend to slide and rotate, i.e. changing the soil fabric, to support the continuous rotation of the principal stress direction. This change in soil fabric results in more loss of contact during normal cycles and consequently induces large amounts of strain in the sample. However, even after 60 cycles of rotation (by the end of the test), the residual deformation (residual strain) occurring in the geogrid reinforcement is negligible

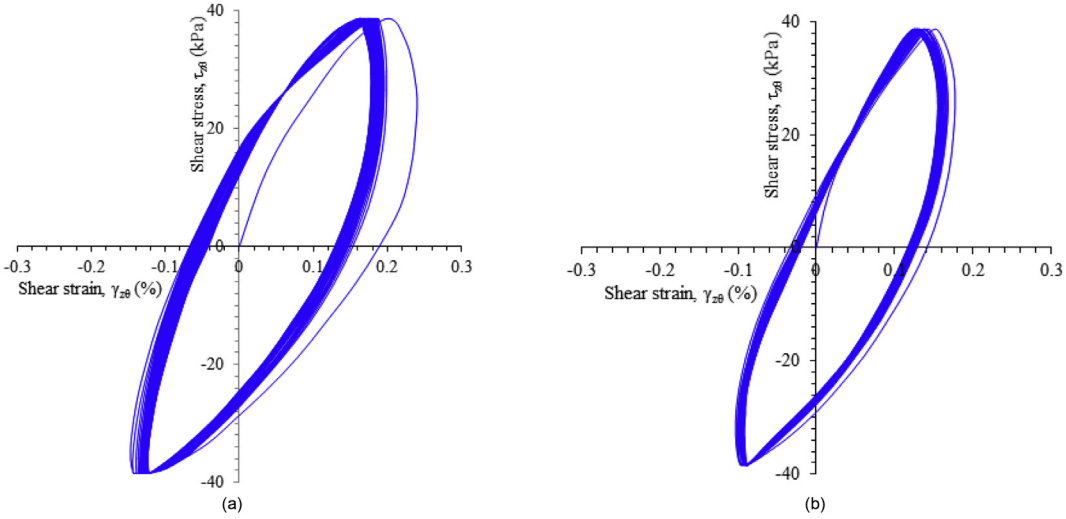

Fig. 17. Hysteretic shear stress–strain relationships for (a) unreinforced sand and (b) 5-layer reinforced sand under cyclic rotation of the principal stress direction.

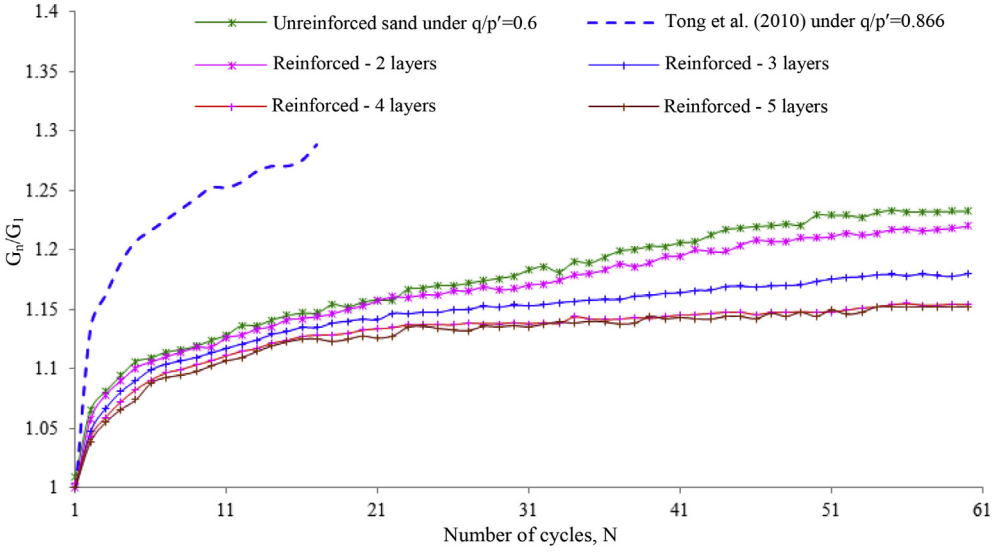

Fig. 18. Variations in the ratio of shear modulus (G_n/G_1) of unreinforced and reinforced sands under cyclic rotation of the principal stress direction.

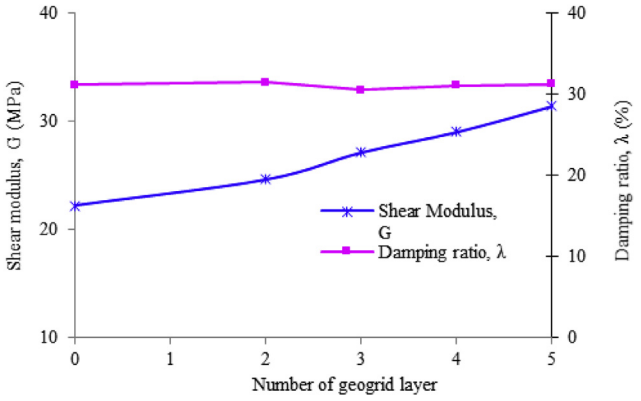

Fig. 19. Variations of shear modulus and damping ratio at the first cycle with number of geogrid layers.

for both cases ($n = 2$ layers and $n = 5$ layers) and thus we could not compute the mobilized stress of reinforcement. This negligible residual strain could be attributed to the nature of the cyclic test conducted to investigate the induced strain of reinforced sand as a composite material under continuous rotation of the principal stress direction while the deviatoric stress is kept constant. In other words, constant deviatoric stress results in a slight amount of plastic strain in reinforcement that is too small to measure. Moreover, this applied constant deviatoric stress is lower compared with the peak deviatoric stress of the soil where unreinforced sand fails under a static deviatoric stress of $q = 112$ kPa (Al-rkaby et al., 2017) while only 60 kPa is applied during this rotational test. Therefore, under such conditions of low and constant deviatoric stress associated with continuous rotation of the principal stress direction, only elastic strain can be mobilized in reinforcement and it then returns back to its original position after a certain number of cycles when removing loading.

This is a step towards extensive studies of the effects of anisotropy on reinforced soil using this advanced apparatus. Under a higher stress ratio, plastic strain in geogrid may be induced.

3.3. Shear modulus and damping ratio

Shear modulus (G) is defined as the secant slope connecting the extreme points on the hysteresis loop (Fig. 16) (Maheshwari et al., 2013). Fig. 17 shows the hysteresis loops inclined to vertical as the number of cycles increases. The largest incline occurs during the first cycle and then decreases. The ratio of shear modulus (G_n/G_1) obtained from subsequent cycles normalized on the shear modulus of the first cycle (G_1) is shown in Fig. 18. It is clear that the shear modulus of unreinforced sand increases by approximately 6.5% during the second cycle, by 10.6% during the 5th cycle, and then the increasing rate decreases until the ratio of shear modulus reaches approximately 117% after 30 cycles and 123% by the end of 60 cycles. This agrees with previous studies of Yan et al. (2015) and Tong et al. (2010), and can be explained by the densification that occurs in the sand during cyclic rotation and also the shear history, as mentioned previously.

The reinforcement results in a clear increase in the shear modulus where it increases in the first cycle from 22.2 MPa for an unreinforced sand to 27.1 MPa, 29 MPa and 31.4 MPa for reinforced sand with 3–5 layers, respectively, as shown in Fig. 19. However, reinforcement with 2 layers exhibits a slight increase in the shear modulus when compared with samples containing 3–5 reinforcement layers. This increase in shear modulus is linked to the restrain and confinement of the geogrid that result in eliminating the induced shear strain.

It can be observed that increasing the reinforcement layers results in significantly increasing the shear modulus during the first cycle and then the increasing rate becomes smaller and stable during the subsequent cycles. For example, the increase in shear modulus after 60 cycles reaches 22%, 18%, 15.4% and 15.2% for 2–5 layers, respectively (Fig. 19). Although there is a low rate of increase during the subsequent cycles, the shear modulus value at the end of 60 cycles of rotation is higher as the reinforcement layers increase where the shear modulus increases by 30%, 31.9%, 33.46% and 36.17% for reinforced sand with 2–5 layers after 60 cycles, respectively.

The damping ratio (λ) refers to the energy dissipated by soil during the cyclic loading (Chen et al., 2016), and can be calculated directly from each hysteresis loop of the shear strain-shear stress relationship (Fig. 16) for each hysteresis loop using $\lambda = \Delta W/(4\pi W)$.

It is found that the damping ratio calculated from the first cycle is kept constant at about 31% without significant change for both the unreinforced and reinforced sands (Fig. 19). This insignificant variation in the damping ratio for both the unreinforced and reinforced sands is related to the damping ratio of the soil which is a function of the loading velocity represented by the frequency of loading during cycles (RaviShankar et al., 2005; Naeini and Gholampoor, 2014). In this study, the frequency of cyclic rotation

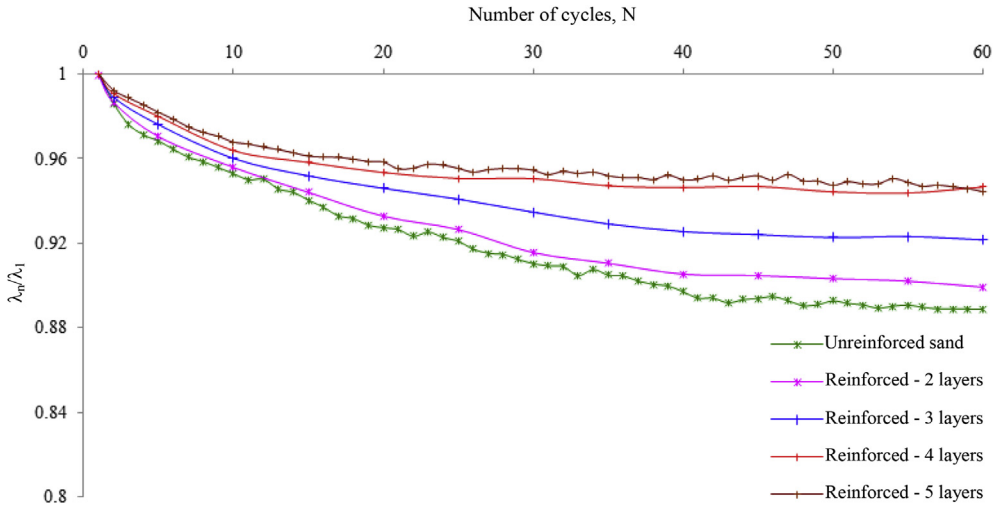

Fig. 20. Variations in the normolized damping ratio (λ_n/λ_1) of unreinforced and reinforced sands under cyclic rotation of the principal stress direction.

is constant and thus the variation in damping ration is insignificant. This is consistent with what reported by Naeini and Gholampoor (2014). However, with increasing number of cycles, damping ratio tends to decrease. For example, the damping ratio of unreinforced sand decreases from 31.14% during the first cycle to 27.64% after 60 cycles, whereas for reinforced sand with 5 layers, it decreases slightly from 31.2% to 29.47% (Figs. 19 and 20). This decrease is linked to the densification occurring due to the cyclic rotation and it is in agreement with the results reported by Uthayakumar (1992) and Kirar and Maheshwari (2013) who demonstrated that decrease in damping ratio and increase in shear modulus are related to the increase in density. It can also be related to that stiff material, obtained due to decreasing void ratio during load cycles, dissipates lower amount of energy during the cyclic load (Uthayakumar, 1992).

4. Conclusions

The large hollow cylinder apparatus (HCA-600) used in this study offers a great opportunity for conducting fundamental research to investigate the cyclic rotation of the principal stress direction. Despite the constant deviatoric stresses during testing, cyclic rotation of the principal stress direction results in significant development of the strain components: vertical (ε_z), radial (ε_r), circumferential (ε_θ) and shear ($\gamma_{z\theta}$) strains. In addition to the effects on shear modulus and damping ratio, these effects of rotation are still important even in the presence of reinforcement. Based on the results and discussion in the previous section, the following conclusions can be drawn:

(1) Periodic variation of the induced strains is observed and most strains occur during the first cycle. With increasing number of cycles, ε_θ and ε_r increase and $\gamma_{z\theta}$ and ε_z decrease moderately and then become constant. Moreover, at the end of each cycle of rotation, these strains are not recovered completely, although the stress state returns back to the initial state, indicating that plastic strains occur.

(2) The oscillation characteristics of the strains are related to the variation of stress components (σ_z, σ_θ and $\tau_{z\theta}$) and also to the continuous rotation of the anisotropic fabric that is associated with the rotation of the principal stress direction.

(3) During the first cycle, $\gamma_{z\theta}$ increases to a maximum value of 0.24% at $\alpha = 70^\circ$, and then decreases to −0.1467% at $\alpha = 145^\circ$, and finally reaches −0.0674% at $\alpha = 180^\circ$. A similar trend is observed for ε_r and ε_θ although the variation is only on the contractive side where ε_r increases to 0.1248% at $\alpha = 120^\circ$, and then decreases slightly to 0.1092% at $\alpha = 180^\circ$; while ε_θ increases to 0.3246% at $\alpha = 105^\circ$, and then decreases to 0.224% at 180°. However, ε_z exhibits dilation behavior where it increases to −0.3915% at $\alpha = 105^\circ$, and then decreases to −0.2567% at $\alpha = 180^\circ$.

(4) The volumetric strain varies significantly during the first five cycles of rotation, and then this variation decreases as the number of cycles increases. The sand exhibits contraction behavior during the first five cycles and after that some dilation also occurs.

(5) The geogrid reinforcement provides confinement and restraint that decrease the strains induced by the cyclic rotation. As the number of reinforcements increases, the restraint increases. With five reinforcement layers, for example, the maximum values of strains during the first cycle of rotation decrease to −0.3398% (for ε_z), 0.2197% (for ε_θ), and 0.1767% (for $\gamma_{z\theta}$) compared with values of unreinforced sand mentioned in the above point (3). Moreover, reinforced samples exhibit lower values of irrecoverable plastic strains. Radial strain (ε_r) has not been affected by reinforcement in the first cycle. However, it decreases significantly during subsequent cycles compared to ε_r of unreinforced sand.

(6) Rotation from 45° to 135° exhibits higher strains compared with other ranges of rotation and this can be related to the samples entering an extension mode during this range, in addition to the relative approach between the mobilized plane and the bedding plane.

(7) Reinforcement appears to have no effect on the damping ratio, while the shear modulus increases as the number of geogrid layers increases.

(8) As the rotation continues, the shear modulus increases while damping ratio decreases for both reinforced and unreinforced sands. This trend is related to the densification which occurs due to increasing cycles resulting in less shear strain, less dissipation of energy and consequently higher shear modulus and lower damping ratio.

Conflict of interest

We wish to confirm that there are no known conflicts of interest associated with this publication and there has been no significant financial support for this work that could have influenced its outcome.

Acknowledgements

Alaa Hussein Jassim Al-rkaby is grateful for the PhD scholarship awarded by the Higher Committee for Education Development in Iraq (HCED) enabling his studies at Curtin University.

References

Al-rkaby AHJ, Chegenizadeh A, Nikraz HR. Directional dependence in the mechanical characteristics of sand: a review. International Journal of Geotechnical Engineering 2016;10(5):499–509.

Al-rkaby AHJ, Chegenizadeh A, Nikraz HR. Anisotropic response of large scale geogrid-reinforced sand to principal stress direction: experimental study. Soils and Foundations 2017. http://dx.doi.org/10.1016/j.sandf.2017.03.008.

Azami A, Pietruszczak S, Guo P. Bearing capacity of shallow foundations in transversely isotropic granular media. International Journal for Numerical and Analytical Methods in Geomechanics 2010;34(8):771–93.

Cai Y, Yu HS, Wanatowski D, Li X. Non-coaxial behavior of sand under various stress paths. Journal of Geotechnical and Geoenvironmental Engineering 2013;139(8):1381–95.

Chandrasekaran B, Broms BB, Wong KS. Strength of fabric reinforced sand under axisymmetric loading. Geotextiles and Geomembranes 1989;8(4):293–310.

Chen G, Zhou Z, Pan H, Sun T, Li X. The influence of undrained cyclic loading patterns and consolidation states on the deformation features of saturated fine sand over a wide strain range. Engineering Geology 2016;204(8):77–93.

Fonseca J, O'sullivan C, Coop MR, Lee PD. Quantifying the evolution of soil fabric during shearing using scalar parameters. Géotechnique 2013;63(10):818–29.

Fu P, Dafalias YF. Fabric evolution within shear bands of granular materials and its relation to critical state theory. International Journal for Numerical and Analytical Methods in Geomechanics 2011;35(18):1918–48.

Guo L, Chen J, Wang J, Cai Y, Deng P. Influences of stress magnitude and loading frequency on cyclic behavior of K_0-consolidated marine clay involving principal stress rotation. Soil Dynamics and Earthquake Engineering 2016;84:94–107.

Habibi MR, Shafiee A, Jafari MK. Monotonic behavior of geotextile reinforced soils under discrete rotation of principal stress. Iranian Journal of Science and Technology: Transactions of Civil Engineering 2014;38(C2):325.

Higuchi T, Ishihara K, Tsukamoto Y, Masuo T. Deformation and strength of geogrid-reinforced granular soil at plane strain conditions. Soils and Foundations 1998;38(1):221–7.

Hosseininia ES. Discrete element modeling of inherently anisotropic granular assemblies with polygonal particles. Particuology 2012;10(5):542–52.

Ishihara K, Towhata I. Sand response to cyclic rotation of principal stress directions as induced by wave loads. Soils and Foundations 1983;23(4):11–26.

Jiang M, Shen Z, Li L, Su J. A novel specimen preparation method for TJ-1 lunar soil simulant in hollow cylinder apparatus. Journal of Rock Mechanics and Geotechnical Engineering 2012;4(4):312–25.

Kirar B, Maheshwari BK. Effects of silt content on dynamic properties of Solani sand. In: Proceedings of the 7th International Conference on case histories in geotechnical engineering. Missouri University of Science and Technology; 2013.
Li X, Yang D, Yu HS. Macro deformation and micro structure of 3D granular assemblies subjected to rotation of principal stress axes. Granular Matter 2016;18(3):1–20.
Li X, Yu HS. Numerical investigation of granular material behaviour under rotation shear. Géotechnique 2010;60(5):381–94.
Li XS, Dafalias YF. Anisotropic critical state theory: role of fabric. Journal of Engineering Mechanics 2012;138(3):263–75.
Liu CN, Yang KH, Nguyen MD. Behavior of geogrid-reinforced sand and effect of reinforcement anchorage in large-scale plane strain compression. Geotextiles and Geomembranes 2014;42(5):479–93.
Liu CN, Zornberg JG, Chen TC, Ho YH, Lin BH. Behavior of geogrid-sand interface in direct shear mode. Journal of Geotechnical and Geoenvironmental Engineering 2009;135(12):1863–71.
Maheshwari B, Kale S, Kaynia A. Dynamic properties of Solani sand at large strains: a parametric study. International Journal of Geotechnical Engineering 2013;6(3):353–8.
Meyerhof GG. Bearing capacity of anisotropic cohesionless soils. Canadian Geotechnical Journal 1978;15(4):592–5.
Miura K, Miura S, Toki S. Deformation behavior of anisotropic dense sand under principal stress axes rotation. Soils and Foundations 1986;26(1):36–52.
Naeini SA, Gholampoor N. Cyclic behaviour of dry silty sand reinforced with a geotextile. Geotextiles and Geomembranes 2014;42(6):611–9.
Nakata Y, Hyodo M, Murata H, Yasufuku N. Flow deformation of sands subjected to principal stress rotation. Soils and Foundations 1998;38(3):115–28.
Nazzal M, Abu-Farsakh M, Mohammad L. Laboratory characterization of reinforced crushed limestone under monotonic and cyclic loading. Journal of Materials in Civil Engineering 2007;19(9):772–83.
Nguyen MD, Yang KH, Lee SH, Wu CS, Tsai MH. Behavior of nonwoven-geotextile-reinforced sand and mobilization of reinforcement strain under triaxial compression. Geosynthetics International 2013;20(3):207–25.
Oda M, Koishikawa I. Effect of strength anisotropy on bearing capacity of shallow footing in a dense sand. Soils and Foundations 1979;19(3):15–28.
Peng FL, Kotake N, Tatsuoka F, Hirakawa D, Tanaka T. Plane strain compression behavior of geogrid-reinforced sand and its numerical analysis. Soils and Foundations 2000;40(3):55–74.
Qin J, Zeng X, Ming H. Influence of fabric anisotropy on seismic responses of foundations. Journal of Rock Mechanics and Geotechnical Engineering 2015;7(2):147–54.
RaviShankar BV, Sitharam TG, Govindaraju L. Dynamic properties of Ahmedabad sands at large strains. In: Proceedings of Indian geotechnical conference; 2005. p. 369–72.
Razeghi HR, Romiani HM. Experimental investigation on the inherent and initial induced anisotropy of sand. KSCE Journal of Civil Engineering 2015;19(3):583–91.
Sazzad MM, Suzuki K. Micromechanical behavior of granular materials with inherent anisotropy under cyclic loading using 2D DEM. Granular Matter 2010;12(6):597–605.
Symes MJ, Gens A, Hight DW. Drained principal stress rotation in saturated sand. Géotechnique 1988;38(1):59–81.
Tatsuoka F, Iwasaki T, Takagi Y. Hysteretic damping of sands under cyclic loading and its relation to shear modulus. Soils and Foundations 1978;18(2):25–40.
Tong Z, Fu P, Zhou S, Dafalias YF. Experimental investigation of shear strength of sands with inherent fabric anisotropy. Acta Geotechnica 2014;9(2):257–75.
Tong ZX, Yu YL, Zhang JM, Zhang G. Deformation behavior of sands subjected to cyclic rotation of principal stress axes. Chinese Journal of Geotechnical Engineering 2008;30(8):1196–202 (in Chinese).
Tong ZX, Zhang JM, Yu YL, Zhang G. Drained deformation behavior of anisotropic sands during cyclic rotation of stress principal axes. Journal of Geotechnical and Geoenvironmental Engineering 2010;136(11):1509–18.
Uthayakumar M. Dynamic properties of sands under cyclic torsional shear [Ph.D. Thesis]. Kelowna, Canada: University of British Columbia; 1992.
Vaid YP, Sayao A, Hou E, Negusse D. Generalised stress-path dependent behaviour with a new hollow cylinder torsional apparatus. Canadian Geotechnical Journal 1990;27(5):601–16.
Wang Y, Wu D, Qiu Y, Wang D. Experimental investigation on cyclic deformation behavior of soft marine clay involved principal stress rotation. Marine Georesources and Geotechnology 2016. http://dx.doi.org/10.1080/1064119X.2016.1194922.
Wang ZJ, Luo YS, Guo H, Tian H. Effects of initial deviatoric stress ratios on dynamic shear modulus and damping ratio of undisturbed loess in China. Engineering Geology 2012;143(8):43–50.
Wijewickreme D, Vaid YP. Behavior of loose sand under simultaneous increase in stress ratio and principal stress rotation. Canadian Geotechnical Journal 1993;30(6):953–64.
Xiong H, Guo L, Cai Y, Yang Z. Experimental study of drained anisotropy of granular soils involving rotation of principal stress direction. European Journal of Environmental and Civil Engineering 2016;20(4):431–54.
Yan JJ, Zhou J, Gong XN, Cao Y. Undrained response of reconstituted clay to cyclic pure principal stress rotation. Journal of Central South University 2015;22(1):280–9.
Yang L. Experimental study of soil anisotropy using hollow cylinder testing [Ph.D. Thesis]. Nottingham, UK: University of Nottingham; 2013.
Yang Y, Fei W, Yu HS, Ooi J, Rotter M. Experimental study of anisotropy and non-coaxiality of granular solids. Granular Matter 2015;17(2):189–96.
Yang ZX, Li XS, Yang J. Undrained anisotropy and rotational shear in granular soil. Géotechnique 2007;57(4):371–84.
Yu HS, Yang LT, Li X, Wanatowski D. Experimental investigation on the deformation characteristics of granular materials under drained rotational shear. Geomechanics and Geoengineering 2016;11(1):47–63.

Alaa H.J. Al-rkaby is currently PhD candidate in Geotechnical Engineering at Department of Civil Engineering, School of Civil and Mechanical Engineering, Curtin University, Australia. He obtained a BSc degree in Civil Engineering from Mosul University. In 2004, he obtained his MSc degree in Geotechnical Engineering from the same University. In addition to his career as a lecturer, Al-rkaby spent some years as the manager of the construction laboratory, and then director of the engineering consultant bureau. He is also an active consultant. The projects in which he acted as designer, consultant or responsible of soil investigations are numerous and concern a variety of topics in structural, geotechnical, and petroleum engineering. E-mail addresses: a.al-rkaby@postgrad.curtin.edu.au; alaa.astm@gmail.com.

Dr. A. Chegenizadeh is working as lecturer in Department of Civil Engineering, School of Civil and Mechanical Engineering, Curtin University, Australia. Dr. Chegenizadeh has published many scientific papers in the geotechnical engineering.

Dr. H.R. Nikraz is a professor at the Department of Civil Engineering, School of Civil and Mechanical Engineering, Curtin University, Australia. Prior to his academic career, he had many years' experience working in industry in the Middle East, Europe and Australia. He has provided numerous consultancy services in his field to over 200 organizations nationally and internationally. He obtained his PhD at Curtin University of Technology in 1989. Dr. Nikraz is a fellow of the Institution of Engineers, Australia. He has guided 80 PhD theses, 35 Master students and published over 500 publications in various journals, books and conference proceedings. Dr. Nikraz has initiated research works in the area of Geotechnics, Geopolymers, Concrete, Soil Stabilization and Pavement Engineering. Dr. Nikraz is also the reviewer of many national and international journals.